Batteries & Supercaps

Research Article
doi.org/10.1002/batt.202400086

Chemistry Europe
European Chemical Societies Publishing

www.batteries-supercaps.org

An Automatized Rebalancing System to Address Faradaic Imbalance and Prolong Cycle Life in Alkaline Ferrocyanide – Anthraquinone Redox Flow Batteries

Miguel Cantera,[a] Lara Lubián,[b, c] Koray Cavusoglu,[c] Rubén Rubio-Presa,[c] Roberto Sanz,[c] Virginia Ruiz,[b, c] Jose María Cámara,*[a] and Edgar Ventosa*[b, c]

Aqueous Organic Redox Flow Batteries are a family of promising energy storage systems. However, they face various challenges related to their lifetime, such as the Faradaic imbalance due to the occurrence of parasitic reaction leading to the fading of its energy storage capacity. Herein, automatization of a rebalancing system to reverse the detrimental effects of Faradaic imbalance due to the unavoidable presence of small quantities of oxygen in the negative reservoir or hydrogen evolution reaction is developed and implemented in an alkaline flow battery. A membrane-free rebalancing cell is proposed to promote the oxygen evolution reaction and reverse the accumulated charge in the catholyte showing a 100% coulombic efficiency. The programmable logic controller monitors the open circuit voltage to calculate the charge stored in each charge/discharge step and closes a circuit so a fixed voltage is applied to the rebalancing cell when the battery needs to be rebalanced. The system is tested using an alkaline flow battery consisting of ferrocyanide and 2,6-dihydroxyanthraquinone, improving the energy capacity retention from 0.27% cycle-1 and 0.47% h-1 without rebalancing system to 100% retention after >850 cycles and >24 days (without Ar-filled glovebox), demonstrating the feasibility of this proposed system to address the Faradaic imbalance.

Introduction

The transition for energy generation from fossil-based systems to renewable energy sources is one of the most important objectives in the political agenda worldwide due to environmental and economic reasons. Unfortunately, the intermittency of these renewable sources hinders the transition since generation and consumption of energy do not always match. In this sense, implementation of energy storage systems plays a pivotal role since they can store the excess of energy generated during periods of abundance in renewable sources, releasing the stored energy during peaks of energy consumption. The balanced performances of batteries make them a growing alternative for energy storage.[1,2,3] Among the various battery technologies, redox flow batteries (RFBs) are especially suitable for stationary energy storage.[4,5,6,7] In contrast to other batteries, energy storing materials are dissolved in the electrolytes, which are stored in external reservoirs. Thus, power is associated with the electrochemical reactor, while energy is related to the external reservoirs providing RFB with the capability for independent scalability of power and energy, which is a great asset for energy storage for the grid. The state-of-the-art RFB is the so-called all-Vanadium flow battery. This battery technology is commercially available delivering suitable performances for stationary energy storage.[8,9,10,11] However, all active species are based on Vanadium, which has been identified as critical material for the U.S.A and Europe for several years. Therefore, the development of redox flow battery technologies based on Earth-abundant elements has being a very intensive field of research in the last years.[12,13] Among the pursued alternatives, RFBs based on aqueous electrolytes and organic electroactive species have received much attention, being referred to as aqueous organic redox flow batteries (AORFBs).[14,15] Several examples of AORFB have shown to deliver promising features, leading to the establishment of multiple startup companies based on AORFB.[8,16] While parameters such as sustainability of the raw materials, energy density, specific power, energy efficiency have been demonstrated to be competitive against all-Vanadium flow battery, effort needs to be devoted to improving cycle stability.[17,18] This parameter is of special importance considering that AORFB are meant to be deployed for stationary energy storage.

[a] M. Cantera, Prof. J. M. Cámara
Department of Electromechanical Engineering
University of Burgos
Avenida Cantabria s/n. E-09006 Burgos, Spain
E-mail: checam@ubu.es

[b] L. Lubián, V. Ruiz, Prof. E. Ventosa
International Research Centre in Critical Raw Materials-ICCRAM
University of Burgos
Plaza Misael Bañuelos s/n, E-09001 Burgos, Spain
E-mail: eventosa@ubu.es

[c] L. Lubián, K. Cavusoglu, R. Rubio-Presa, Prof. R. Sanz, V. Ruiz, Prof. E. Ventosa
Department of Chemistry
University of Burgos
Plaza Misael Bañuelos s/n, E-09001 Burgos, Spain

Supporting information for this article is available on the WWW under https://doi.org/10.1002/batt.202400086

Fading of energy storage capacity upon cycling for AORFBs (cycle stability) is driven by several mechanisms. The (electro−)chemical stability of active species is the first parameter to be studied in the development of new types of AORFBs. Many molecules have shown so far to be extraordinarily stable, with many strategies reported to improve this challenge.[17,19] Crossover of active species through the membrane that confines each active species in its corresponding compartment also plays an important role. There are several approaches to address this challenge.[20] For all-Vanadium flow batteries, crossover has a large impact in capacity retention in the short-term. Fortunately, this imbalance can be addressed by electrolyte remixing, so that the process is reversible. However, the occurrence of irreversible electrochemical side reactions such as hydrogen evolution reaction (HER) also contributes to capacity fading,[21,22] being referred to as Faradaic Imbalance.[23] The importance of the Faradaic imbalance is that its effects in the capacity retention are irreversible, and it cannot be restored by electrolyte reflowing or remixing. Thus, even if its magnitude per cycle is small, its accumulative nature results in a major challenge for the long-term. In particular the oxygen reduction reaction (or the reaction of oxygen with "charged" anolyte) is a challenge that is surprisingly often neglected, as pointed out in previous works.[24,25] From an academic perspective, Faradaic imbalance associated with oxygen is addressed by introducing the RFB system in an Ar-filled glovebox.[26,27] Unfortunately, this approach is not effective for large scale deployment. It should be noted that complete sealing of a very large flow systems is quite challenging. This issue is not intrinsic to AORFB, but also occurs in other types of RFB. For instance, several strategies have been proposed for reversing Faradaic imbalance for all-Vanadium flow battery,[28,29] since capacity fading and its rebalancing affects critically the cost of any RFB.[30] Overall, there are two types of rebalancing approaches: chemical and electrochemical methods. In both cases, the methods aim at reducing charges accumulated in the catholyte due to the irreversible reduction oxygen taking place in the anolyte. In the former, a reducing chemical agent is added to the catholyte,[31] while the latter is based on direct electrochemically reduction. By implementing the latter approach, our group demonstrated that charge-balanced AORFBs can be continuously cycled for many weeks without Ar-filled glovebox. However, reduction of ferricyanide accumulated in the catholyte during oxygen reduction in the anolyte requires a counter reaction, which in the proposed strategy was the oxygen evolution reaction in the catholyte. In other words, the oxygen evolution reaction was promoted to compensate the effects of the opposite reaction (oxygen reduction reaction) in the opposite compartment (anolyte). As pointed out in this work, the oxygen evolution reaction inside a standard electrochemical reactor will certainly limit the lifespan of the reactor by corroding the carbon electrodes. In parallel, Adeas et al proposed an effective strategy for practical deployment of this electrochemical methods for all-Vanadium flow battery, which is based on decoupling the rebalancing reaction in an external reactor.[32] By doing this, the rebalancing electrochemical device can be specially designed for this purpose, e.g. replacing carbon-based positive electrode by non-corrosive materials, or even replace only this device in the long-term.

The Faradaic imbalance due to parasitic reactions in the anolyte may be triggered by three mechanisms. I) The small entry of air in the anolyte. II) Hydrogen evolution reaction (HER) for active species having a low redox potential. And III) degradation of active species during charging process, e.g. dimerization of the dihydroxy anthraquinone (DHAQ).[20,33] Regardless of the mechanism, the occurrence of the parasitic reaction in the anolyte results in an accumulation of charged active species in the catholyte, which reduces the available of active species in the catholyte.

In this work, automatization of the rebalancing process for reversing Faradaic imbalance is developed demonstrating the practical value of this approach to pave the way for AORFBs to become competitive technologies for stationary energy storage. The entry of oxygen is used as case study but the approach is valid for the other cases, e.g. HER. A new rebalancing device for use in alkaline media is fabricated to enable decoupling of electrochemical rebalancing based on the promotion of the oxygen evolution reaction in an external device in the catholyte circuit. Implementation of a programmable logic controller (PLC) and other electronic components in the system to automatize the process is described in this work enabling continuous operation for several weeks without any significant capacity fading.

Results and Discussion

Capacity Fading in Alkaline Flow Batteries based on Ferrocyanide

While the capacity fading of ferrocyanide in alkaline media is an ongoing debate,[18,19,34] the latest results indicate that self-discharge of ferricyanide provoking oxygen evolution reaction leads to capacity decay in symmetrical cell (cell having ferrocyanide in one side and ferricyanide in the other side).[18] This mechanism would explain why capacity decay is observed only sometimes since it depends on several factors, e.g. oxygen pressure (inside or outside an Ar-filled glovebox), the catalytic properties of the carbon felt. Thus, the self-discharge of Fe^{3+} to Fe^{2+} may indeed lead to a capacity fading in symmetrical cells. We evaluated the self-discharge rate of ferricyanide inside and outside the Ar-filled glovebox using a symmetrical cell (0.1 M $K_3Fe(CN)_6$ + 0.1 M $K_4Fe(CN)_6$ in 1 M KOH for both compartments). Figure S1 shows that the capacity in the experiment inside the glovebox starts to decay after 300 cycles (3.5 days). This is the time required to consume the excess placed in the counter-electrode (20 mL versus 10 mL). Then, the capacity decay is approx. 5% day^{-1}. Outside the glovebox, the same excess was not consumed after 5 days, and the capacity decay was small. This shows that the self-discharge is decreased outside the glovebox. To quantify the differences, specific experiments were carried out (Figure S2). The symmetrical cell was cycled (5 cycles), then it was fully charged and left at open circuit for 12/24 h. It should be noted that the duration of OCV

Research Article
doi.org/10.1002/batt.202400086
Chemistry Europe
European Chemical Societies Publishing

was adjusted to obtain comparable Coulombic efficiencies and make the results more comparable (self-discharge is higher at higher state of charge). The difference between the Coulombic efficiency in the previous cycle and the cycle in which open circuit was applied indicates how much of the ferricyanide was spontaneously reduced to ferrocyanide at full state of charge. This measurement indicated a self-discharge rate of 12% day^{-1} and 4% day^{-1} inside and outside the Ar-filled glovebox, respectively. This observation is consistent with Aziz's work, and it is attributed to the thermodynamic shift of the redox potential for oxygen evolution reaction in the absence of O_2.[18]

These experiments were performed in a symmetrical cell. However, capacity fading of the full battery will depend on the differences between the self-discharge rate occurring in the positive and negative compartment. If the self-discharge rate for catholyte and anolyte are the same, they will cancel out and the capacity fading will not occur. Otherwise, the capacity fading of the full cell will be determined by the side having higher self-discharge rate. In the case of the anolyte, self-discharge will be triggered by 2 reactions; the presence of oxygen (reduction of oxygen and oxidation of charged anolyte) and the evolution of hydrogen (charged anolyte oxidizes leading to the reduction of water). When the presence of oxygen is prevented by working inside the glovebox, the self-discharge rate for anolyte will be minimized since it will only depend on the hydrogen evolution reaction. Thus, we quantified the self-discharge rate of fully charged dihydroxi-anthraquinone (DHAQ) anolyte following the same procedure used for the catholyte (Figure S3) inside an Ar-filled glovebox. An oversize positive compartment containing 40 mL 0.1 M $K_3Fe(CN)_6$ + 0.2 M $K_4Fe(CN)_6$ in 1 M KOH was employed to ensure that the capacity is attributed to the negative compartment (12 mL 0.2 M DHAQ in 1 M KOH). Indeed, the capacity fading during standard operation was negligible. The reversible loss of capacity during the cycle in which open circuit was applied leads to a Coulombic efficiency of 91% for 12 h of open circuit. This leads to a self-discharge rate of 18% day^{-1} for DHAQ inside the glovebox. Therefore, the capacity fading of a ferricyanide – DHAQ battery in alkaline media will be dominated by the self-discharge of the anolyte since it is higher (18%) that that of the ferricyanide (12%) inside an Ar-filled glovebox. It should be considered that the inevitable small leaking of oxygen outside the glovebox will further increase the self-discharge rate of the anolyte.

In short, self-discharge of ferricyanide in alkaline media leads to a capacity fading in a symmetrical cell. However, the higher self-discharge rate of the DHAQ in alkaline media provokes that the capacity fading of the full battery is dominated by the self-discharge in the anolyte. As a consequence, ferricyanide is accumulated upon cycling. This explains that our previous approach that consists in the intentionally promoted oxygen evolution reaction by shifting the cut-off voltage to 2.0 V led to prevention of the capacity fading.[35] However, the corrosion of carbon in the electrochemical reactor is a significant concern that requires decoupling this reaction into a separate device, which is called here rebalancing cell.

Rebalancing Device

Faradaic imbalance due to the unavoidable presence of oxygen in the negative reservoir of redox flow batteries is a serious challenge that must be addressed for its large-scale deployment. The irreversible consumption of charges in the anolyte during the charge process prevents the anolyte from reaching full charge state, while the catholyte will be fully charged at the end of the charge process. The discharge process will be then limited by the anolyte, as it was not fully charged. At the end of the discharge, anolyte will return to the initial state of charge, while the catholyte will not be able to fully discharge leading to the accumulation of charge species (Figure 1). These charged species will reduce irreversibly the energy storage capacity of the redox flow battery. Traces of oxygen will slowly but constantly enter the flowing system. While Faradaic imbalance in one single cycle may be perceived as negligible, accumulation of charged species in the catholyte upon hundreds of cycles and thousands of working hours will result in an irreversible capacity fading of the battery.

For alkaline AORFB, our group proposed the promotion of oxygen evolution in the positive electrode since this process enables complete charging of the anolyte as well as rebalancing pH increase caused by oxygen reduction.[35] However, long-term operation may be limited by corrosion of carbon-based electrodes. Alternatively, Poli et. al proposed an elegant strategy for rebalancing an all-Vanadium flow battery – wherein reduction of accumulated charges was achieved using an external device (regeneration cell), connected to the catholyte circuit that resembled the architecture of a filter-pressed redox flow cell.[32] Herein we propose the combination of both rebalancing strategies. That is, reduction of accumulated charges is carried out by promoting the oxygen evolution reaction and electrochemical reduction of ferricyanide using an external device. Noteworthy, our rebalancing cell does not contain ion-selective membrane (lower cost) neither graphite felts (avoid pressure drop). As shown in Figure 2A, the device contains two asymmetric electrodes: a large area expanded graphite where

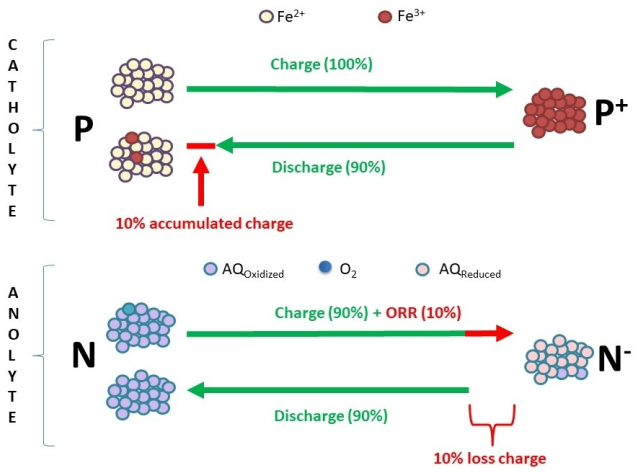

Figure 1. Scheme illustrating the mechanism of Faradaic imbalance in a redox flow battery due to the presence of oxygen in the anolyte.

Research Article
doi.org/10.1002/batt.202400086
Chemistry Europe
European Chemical Societies Publishing

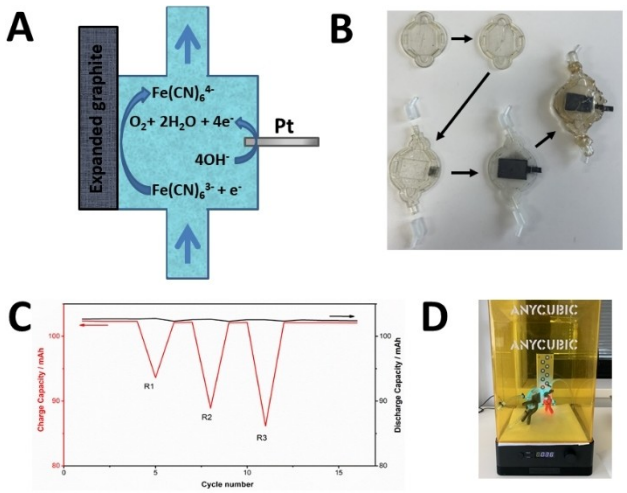

Figure 2. (A) Diagram of the reactions occurring in the rebalancing device when the fixed voltage is applied. (B) Assembling steps of the different parts of the rebalancing device and a fully assembled one already used in an experiment. (C) Evolution of the Coulombic efficiency of the device during cycling with the application of a fixed voltage at three different moments (R1, R2 and R3 with 1 V, 1.2 V and 1.4 V respectively). Catholyte: 13 mL of 0.3 M potassium ferrocyanide in 1 M KOH, anolyte: 45 mL of 0.1 M ferrocyanide and 0.2 M ferricyanide in 1 M KOH. (D) Rebalancing device in the UV curing chamber during the final manufacturing step in the lab.

ferricyanide reduction of takes place, and a smaller area Pt electrode where oxygen evolution reaction takes places. The lack of an ion-selective membrane may induce recombination, as ferrocyanide generated at the expanded graphite can be re-oxidized to ferricyanide at the Pt electrode. In other words, oxidation of ferrocyanide can complete with oxidation of water.

However, if the Pt electrode is significantly smaller than the counter-electrode that is used to reduce ferricyanide, the current density at the Pt electrode will be very large favoring the oxygen evolution reaction due to mass transport limitations. To validate this hypothesis, a rebalancing cell was fabricated using 3-D stereolithography printing (Figure 2B), cured in an ultraviolet curing chamber (Figure 2D) and connected to a redox flow cell to evaluate the coulombic efficiency of the rebalancing process (Figure 2C). The measurement consisted in oxidizing completely the ferrocyanide to ferricyanide in the positive compartment of a symmetrical cell (charging step). Then the circuit was opened for 20 minutes, followed by the reduction (discharging step) at constant current. The charge for the charging and discharging steps was very similar for each cycle, and close to the theoretical value. This indicates that self-discharge does not occur during the open circuit step. After 10 cycles, a bias of 1.0 V was applied to the rebalancing cell during the open circuit step so that part of the ferricyanide was reduced back to ferrocyanide (R1). Then, 4 standard cycles without activation of the rebalancing cell were carried out, followed by one cycle activating the rebalancing cell by applying a bias of 1.2 V (R2). The same procedure was repeated for a bias of 1.4 V (R3). The charge obtained for the discharge step after activation of the rebalancing cell was lower than the values recorded in previous cycles. And the higher the bias applied to the rebalancing cell, the higher the loss observed in the battery capacity. This indicates that ferricyanide is effectively reduced at the rebalancing cell, the amount increasing with applied bias. Considering that oxidation of water might complete with oxidation ferrocyanide generated during the rebalancing process, the ferrocyanide generated in the rebalancing cell might not be proportional (Faradaic constant) to the charge spent in this process. Comparing the charge spent in the rebalancing process and the capacity loss in the battery, the coulombic efficiency of the rebalancing cell can be estimated. The charge spent by the rebalancing cell was 8.3, 13.1 and 15.9 mAh (Figure S4) for 1.0, 1.2 and 1.4 V bias, respectively. And the loss in capacity in the symmetrical cell was 8.5, 13.2 and 15.9 mAh for 1.0, 1.2 and 1.4 V bias, respectively. As a result, the coulombic efficiency for the reduction of ferricyanide was 102, 101 and 100%, which indicates that the membrane-free rebalancing cell is very efficient in the studied range (1.0–1.4 V). The values above 100% are attributed to small errors in the estimation of charge, with larger values leading to lower errors. The energy cost for rebalancing would be 1:1. In other words, if a battery lost 1 kWh after a given period of time, rebalancing the battery to its original capacity would cost around 1 kWh since the coulombic efficiency is 100% and the cell voltage of the rebalancing cell is similar to the nominal one-cell voltage of the battery.

Importantly, we evaluated whether the rebalancing cell reduces Fe^{3+} to Fe^{2+} or oxidises Fe^{2+} to Fe^{3+}. We already observed in our previous measurements for the Coulombic efficiency of the system that the rebalancing cell reduces Fe^{3+} to Fe^{2+}, but we carried out a control experiment to unambiguously demonstrate that the rebalancing cell reduces $Fe^{3+}$to Fe^{2+}. An electrolyte containing 50% Fe^{3+} and Fe^{2+} was circulated through the rebalancing cell without the rest of the system (without electrochemical reactor). Then, we turned on the rebalancing cell for 1 h. After that time, we performed cyclic voltammetry in the electrolyte and compared it with the initial electrolyte using a microelectrode that provides unambiguous results. Figure S5 clearly shows that Fe^{3+} was reduced to Fe^{2+} by the rebalancing cell (anodic current increased afterwards since there is more Fe^{2+} to be oxidized).

Automatization of the System

A PLC is proposed to provide a loop to control automatically the system, formed by the redox flow battery and the rebalancing device. Figure 3A shows a general schematic of the full set-up. The PLC acts as the main part by performing the three following tasks: a) it reads the input: the open circuit voltage (OCV) from the battery by converting the signal from analog to digital, b) it processes the signal by using certain logic to detect the charge imbalance and c) it acts towards an output: the digital relay of the circuit connected to the rebalancing device to recover the capacity of the battery. In other words, the PLC will determine the state of health of the redox flow battery and will trigger the application (switching on/off) of the rebalancing cell when it estimates that electrolyte

Research Article
doi.org/10.1002/batt.202400086
Chemistry Europe
European Chemical Societies Publishing

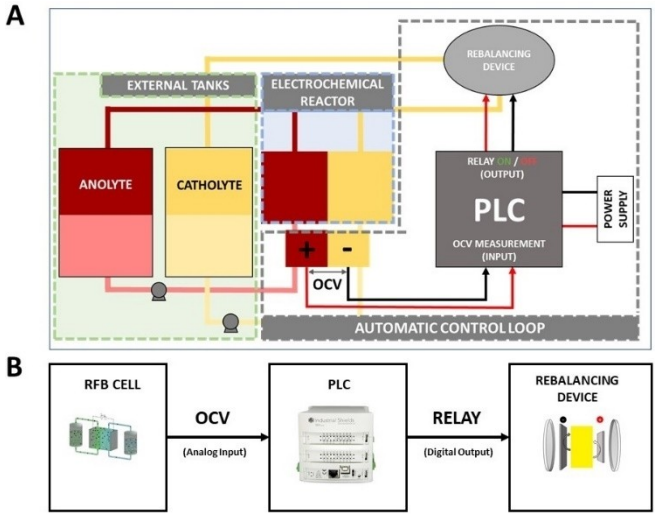

Figure 3. (A) Simplified diagram of an RFB with the proposed rebalancing device controlled by a PLC. (B) Input/Output flowchart of the proposed electronic control loop system.

rebalance is required. Figure 3B shows the input/output flowchart of this process. An M–Duino 38R from Industrial Shields was selected in order to keep the cost of the system low and to have high flexibility. This PLC is based in Arduino platform, it can be powered by a 12–24 V power source and features a 10 V Input/Output module design to work in industrial environments. Besides, it includes several communication protocols so that the PLC can be connected to additional electronic components. This allows the system to improve its performance or add other functionalities.

For the estimation of the state of health of the battery, a real time measurement of the open circuit voltage of the flow battery has to be performed. For this work, a requisite to obtain at least 1 mV accuracy in the reading is set. Although the Arduino Mega board integrated in the PLC includes an analog to digital converter (ADC) embedded in its microcontroller, it has low resolution (only 10 bit) and is limited in configuration options. In order to obtain a signal with more resolution, an external dedicated ADC was selected, specifically the ADS1115 by Texas Instruments, mounted in a break-out board by the manufacturer Adafruit. This ADC has 16-bit resolution, low cost and is suitable to measure low frequency signals like the direct current (DC) voltage of an electrochemical battery. However, only 15-bit are used for values as one is reserved for the sign (positive or negative). The resolution can be calculated by the following expression:

$$resolution\ (volts) = \frac{V_{ref}}{2^n}$$

Where V_{ref} is the reference voltage, which can be set in the Programmable Gain Amplifier of the ADC by software from a list of fixed values and shall be configured depending on the input signal range to avoid signal truncation. For this set-up it has been selected 2.048 V as it is a higher nearest value than the maximum OCV coming out from this RFB and closes. Since the other term n is the number of resolution bits (15), the resolution value obtained is 0.125 mV, achieving the requisite value set before. As this ADC is compatible with I2C protocol it can be connected directly to the PLC. The ADC is powered by 5 V using a DC/DC converter, which is fed by another 24 V power supply. Apart from the resolution, the other important configuration of the ADC is the inputs selection. As the OCV will be read as the differences between its two poles (positive and negative), two differential inputs of the ADC will be used, namely A0 and A1. It is important to note that ADS1115, as a delta-sigma ADC, requires common-mode voltage range to assure that the input voltage values are between ground and the ADC power supply voltage. This implies that the analog ground shall be connected to the battery negative pole, and so, also to the negative selected input of the ADC, A1. Finally, a digital isolator (ADUM1250) is placed between the PLC and the ADC to separate the analog/digital ground paths. Without it, a current loop is created that falsifies the OCV readings, involving a large loss in the measurement accuracy. A breadboard is used to connect all the electronic components. Figure 4 shows the schematic of the complete electronic set-up used for the automatic rebalancing system, where the digital isolator

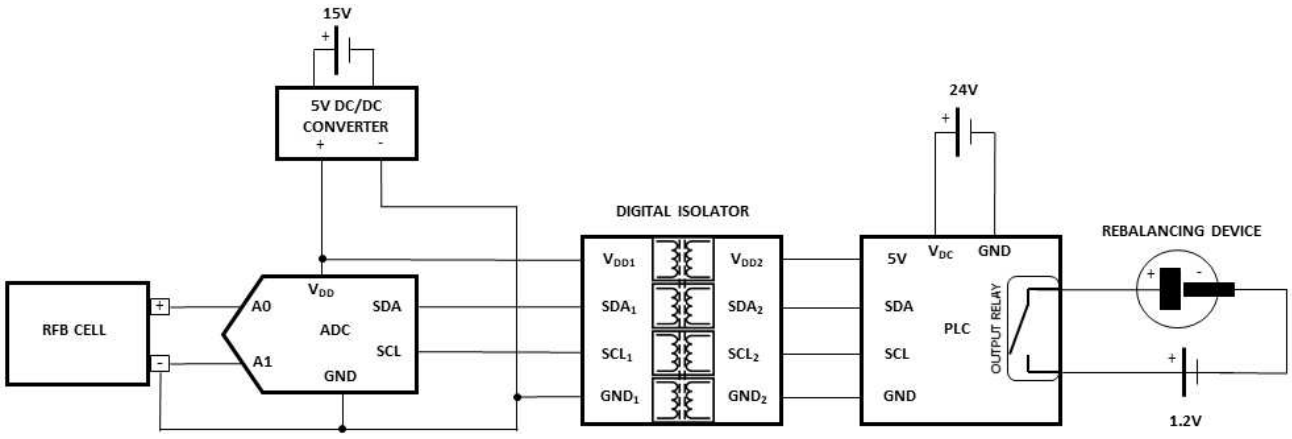

Figure 4. Complete electronic schematic of the control loop for the automatized rebalancing system.

Research Article
doi.org/10.1002/batt.202400086
Chemistry Europe
European Chemical Societies Publishing

separates the analog side (left part) from the digital side (right part). Once the OCV is available as a digital input signal to the PLC, some signal processing is performed. In the loop code part, the OCV values are stored temporary every 0.5 seconds and an average of the values is performed every 2 seconds. The reason for the average computation is to act as a low pass software filter, which removes noise by flattening the signal,[36] avoiding the need to add other electronic components in the set-up. Specifically, it is a finite impulse response filter with equal weights, also called frequency-domain sync filter, with a cut-off frequency of ≈0.2 Hz. The final OCV value is printed out to the Arduino serial monitor and simultaneously saved to a text stored permanently in the hard disk memory of the PC where the PLC is connected to by USB cable. The reason to print the OCV every 2 seconds is having the same number of values per time as the battery test system (BTS) OCV reading which is used as a reference. Once the OCV signal is already processed, the logic to compute the state of health is defined. It has been divided in two functional parts. The first part is the computation of the charge/discharge periods, which is performed by doing an approximated Coulomb Counting. Firstly, the logic detects whether the OCV is increasing constantly over time (charging) or decreasing constantly over time (discharging) so that the duration of each charge/discharge cycle can be determined and stored in memory as T_{ch} and T_{dch} respectively. Initially, the algorithm to calculate these periods was implemented by differentiation in time of two consecutive OCV measurements. However, due to small oscillations in the readings, to avoid false positives, the algorithm was changed to avoid false positives in the following way (similar to the cut-off operation of the BTS): if the PLC reads two consecutive OCV values higher than 0.5 V (always starting with the BTS doing a charge cycle), then it considers that the battery is in charging state; on the other hand, when the OCV reaches 1.42 V, then the battery is considered to be immediately changing to a discharge cycle and hence the PLC changes to discharging state. When these transitions are detected, the timer counting is stopped and the corresponding time value in seconds is stored. As the current density applied by the battery cycler is constant (±30 mA cm^{-2}), the duration of the charging/discharging periods is directly related to the charge storage capacity and thus to the state of health. For instance, a 20% decrease in the charging/discharging periods will translate in a 20% decrease in the charge storage capacity and thus a 20% decrease in the state of health of the battery. Figure 5A shows an example of the evolution of the OCV monitored by the PLC during two consecutive cycles (one charge and one discharge). The second part of the state of health determination logic decides whether the battery is in an imbalanced state or not. The criterion selected is to compare the T_{ch} of the initial cycle (stored as the reference cycle) against the T_{ch} of the current cycle:

$$Imbalance \leftrightarrow T_{ch}(current\ cycle) < p \cdot T_{ch}(reference\ cycle)$$

Where p is a fraction of unity that can be configured in the code and is set in the experiment to 0.8. This means that if T_{ch} of the current cycle gets 0.8 times smaller than T_{ch} of the reference cycle (20% capacity fading), then the battery is considered in imbalanced state and so the rebalancing device shall be activated.

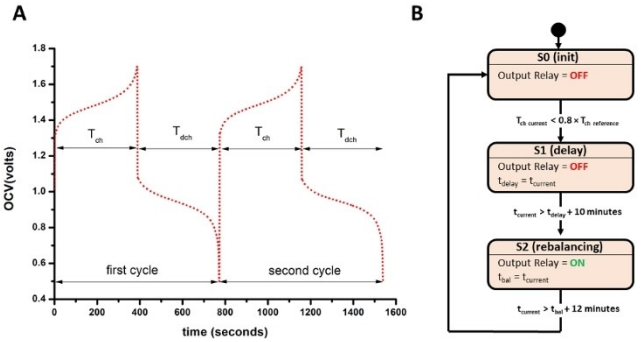

Figure 5. (A) OCV value reading over time during 2 consecutive cycles, where charge and discharge cycles are detected by the PLC and stored in memory. (B) Rebalancing process state machine related with the activation of the output relay.

Finally, the rebalancing device shall be activated so the initial capacity can be restored. As commented before, fading of the charge capacity due to Faradaic imbalance can be reversed by applying a fixed voltage to the external rebalancing device. As shown in the right part of the Figure 4, the PLC will perform this task by controlling the opening/closing (OFF/ON) of one of its digital output relays so that the rebalancing device will be biased by a 1.2 V power supply enabling the rebalancing process to take place. The switching process includes some hysteresis, which means that the relay will be opened if the percentage difference is again above the same percentage limit and will be closed again consecutively when the limit is below, and so on. The 1.2 V bias to the rebalancing device is applied by the same power supply used to feed the DC/DC converter but through a separated channel and circuit. Besides, when an imbalance situation is detected, the relay is not activated immediately so that the bias voltage is applied at the next charge cycle. Then the relay is kept closed during certain fixed time so as the rebalancing process takes some time. In order to simplify and organize the rebalancing process code, a state machine is programmed in the PLC. This state machine has 3 states: S0 (the initial state), S1 (delay, set to 10 minutes) and S1 (balancing, set to 12 minutes). Only S1 closes the digital isolated output relay R1.8 of the PLC, which is connected internally to the Arduino Mega digital output pin 42 Figure 5B shows the state machine diagram performed by the PLC logic, which specifies what happens in each state and how the conditional transitions between states happen. The complete PLC program source code and the ADC software configuration values are included in the Supporting Information, section S3.

Implementation in Anthraquinone – Ferricyanide Flow Battery in Alkaline Media

An alkaline anthraquinone – ferrocyanide redox flow battery was selected to evaluate the proposed strategy. Figure 6 shows a photograph of the full system, which contains 15 mL of 0.2 M 2,6-DHAQ in 1 M KOH and 13 mL of 0.3 M $K_4Fe(CN)_6$ in 1 M KOH as anolyte and catholyte, respectively.

The open circuit voltage (OCV) of the system is continuously monitored by the PLC. As the OCV values change from continuously increasing to continuously decreasing, and vice versa for the discharge process, the PLC can determine the charge stored for each charge and discharge cycle, and compare it with a reference value to assess the state-of-health.

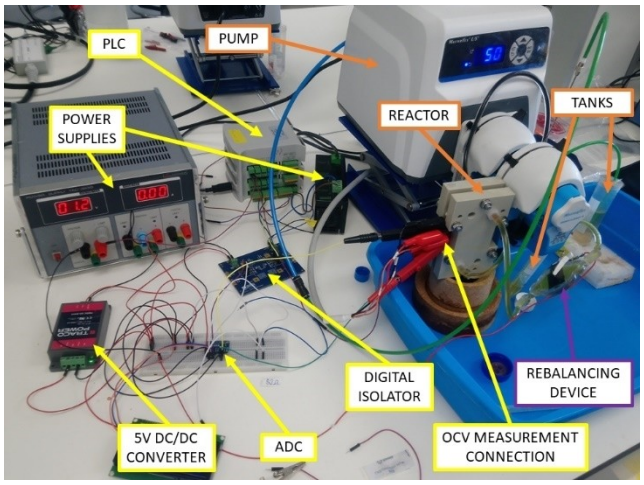

Figure 6. Photograph of the full automatized rebalancing system and the flow battery in operation.

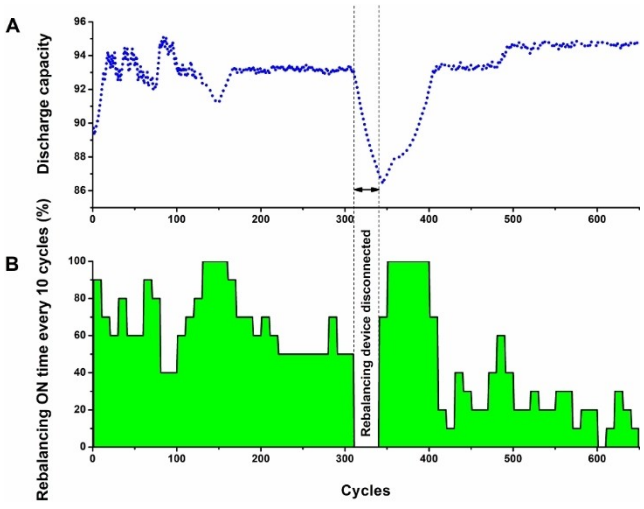

Figure 7. (A) Evolution of the specific discharge capacity of the redox flow battery along the experiment. (B) Evolution of the time percentage that the rebalancing device is activated, shown every 10 cycles. The battery was charged/discharged at constant current (30 mA cm^{-2}) using 1.6 V and 0.5 V as upper and lower cutoff voltages. The rebalancing system was disconnected for 25 cycles between the cycles 300–350. Total operation time was 406 h. Catholyte: 13 mL of 0.3 M potassium ferrocyanide in 1 M KOH, anolyte: 15 mL of 0.2 M 2,6-DHAQ in 1 M KOH.

The catholyte is slightly limiting (less active species than in the anolyte), and determines the maximum practical capacity of the battery, which is estimated to be 100 mAh (utilization rate of 96% of the theoretical value of 104.5 mAh).

Since our goal is to maintain the RFB operating above 95% of its maximum practical value, the PLC will apply the fixed voltage to the rebalancing cell when the charge storage capacity undergoes a 5% decrease in its charge storage capacity. The evolution of the capacity upon cycling (Figure 7a) shows that the capacity initially increased and stabilized at around 93–94 mAh. It should be noted that coulombic efficiency in the first cycle was ca. 90%, hence the rebalancing system is intensively needed during the first cycles. Indeed, the rebalancing system is activated in 9 out of the 10 first cycles (Figure 7b). Afterwards, the rebalancing system was activated less frequently as the levels of oxygen should have decreased after 100 cycles, reaching an activation frequency of 4 out of every 10 cycles (100 cycles). After 130 cycles, the capacity started to decrease gradually, which forced the rebalancing to be activated continuously for 30 consecutive cycles. This could be attributed to a pressure drop in the Ar line due to a significant decrease in temperature. To ensure the absence of air, a small flow of Ar was applied to the reservoir. Ar first goes through a bubble trap where Ar is humidified, also helping us to estimate the flow rate. We observed small changes in the flow rate in this experiment depending on the temperature. Since the overpressure was so small, large changes in temperature could affect the Ar pressure at different points ($PV = nRT$). While this point remains unresolved, the undesired effect of this unexpected event was reversed automatically by the rebalancing system, highlighting the importance of automatization. After 300 cycles, the rebalancing system was manually disconnected (disconnecting the cable of the power source) to evaluate the evolution of the charge storage capacity of the battery without the rebalancing system. A gradually decrease in capacity was observed which is attributed to faradaic imbalance due to oxygen leakage into the negative compartment. After 25 cycles without rebalancing system, the cables were reconnected. Automatically, the rebalancing system was activated. Indeed, the rebalancing system was activated continuously during 50 cycles to reverse the situation and recover the initial value of charge capacity. For the last 250 cycles, the system should have totally consumed all oxygen and the rebalancing system should only reverse the effect of entering oxygen. As a result, the frequency for activation of the rebalancing system decreased to 2–3 out of every 10 cycles, which indicates that oxygen leakage into the negative compartment was small. The tubes broke after 650 cycles, therefore another demonstrator was assembled (Figure S6). The charge capacity for the new demonstrator was maintained during 888 cycles and 24.19 days without any capacity fading (without Ar-filled govebox).

Additionally, the negative compartment was manually aired to simulate an eventual large leakage. The rebalancing system automatically detected and corrected the effect of opening the negative compartment. It should be noted that this battery operated outside an Ar-filled glovebox without rebalancing system (Figure S6b) suffered from a capacity fading of 30% in

110 cycles and 63.82 hours (capacity retention of 0.27% cycle^{-1} and 11% day^{-1}).

Our method can be also useful to prevent degradation of anolytes that is accelerated in the complete absence of oxygen. The DHAQ is a good example. This compound is known to be regenerated in the presence of oxygen.[20] Thus, a small entry of air could be intentionally allowed to prevent dimerization while our method reverses the Faradaic imbalance resulting of the entry. In the case of DHAQ, the electrochemical method proposed by Aziz et al.[33] may be more convenient, but there may be other molecules that cannot be electrochemically regenerated and require reaction with oxygen. Thus, our method can be useful at lab scale since currently there are only two options to evaluate the intrinsic chemical stability. I) the use of an Ar-filled glovebox. This is the best option but all labs do not have it, and it may accelerate the degradation of certain compounds such as DHAQ. II) The use of a large excess of catholyte. In this case, long-term imbalance of the pH value may result in accelerated degradation. Thus, the method proposed here is a third option which can be considered when i) redox species degrade faster in the complete absence of air, e.g. DHAQ or long-term pH changes can affect the stability of the compounds, ii) the redox potential of the active species is very negative leading to the occurrence of HER, and iii) complete sealing of the flow systems is not achieved

The rebalancing system not only balances SOC, but it also balances the pH changes due to the occurrence of irreversible side reactions in the anolyte. It should be noted that the pH change per cycle is very small. To illustrate this, let's assume that the system needs to correct a 0.5% loss of the capacity (e.g. 10 mL of 0.3 M $K_4Fe(CN)_6$ in 1 M KOH). In this case, the capacity would be 80 mA, so that 0.4 mAh should be recovered. Through the Faradic constant, we obtain that 0.015 mmol of H^+ would be released, which results in 0.0015 M. Thus, the concentration of KOH would be reduced from 1.0 M to 0.9985 M, which is not expected to trigger accelerated degradation

Regarding energy cost of the rebalancing system, it is estimated that the energy consumed by the rebalancing system will be similar to the energy to be recovered. This is due to the fact that high Coulombic efficiencies are measured ($>95\%$) and the operating cell voltage (1.2 V) that was applied to the system is similar to the cell voltage of the battery. That is, if the rebalancing system recovers 1% of the capacity, the energy cost would be 1% of the energy capacity of the system. Since our technique is supposed to correct small deviations, we consider that the round-trip efficiency of the system per cycle will not be significantly affected (less than 1%).

Finally, it is worth noting the extraordinarily high capacity retention (100%) over 3 weeks, indicating that ferrocyanide seems to be electrochemically stable in alkaline media in our system.

Conclusions

Faradaic imbalance due to the unavoidable presence of small quantities of oxygen in the reservoirs of RFB operated outside Ar-filled glovebox represents a major challenge for large-scale deployment of AORFBs. In this work, automatization of an electrochemical rebalancing system based on promoting the opposite reaction in the opposite compartment (oxygen evolution reaction in the catholyte) was developed and implemented in an alkaline AORFB to reverse the detrimental effects of Faradaic imbalance. The entry of oxygen was used as case study but the approach is valid for the other cases, e.g. HER. A membrane-free rebalancing cell was designed, and its coulombic efficiency was shown to be of ca. 100%. Its simple design not only reduces costs but also avoids significant pressure drops for electrolyte circulation. A programmable logic controller (PLC) was introduced to control all electronics elements required for the rebalancing system. The PLC monitored the open circuit voltage (OCV) to determine the charge capacity of the battery and analyze whether the rebalancing cell should be activated. When needed, the PLC switched on a relay, enabling powering of the rebalancing cell through a power source (application of a constant bias of 1.2 V). If the charge capacity was increased above a reference value manually coded in the PLC (80% of the theoretical capacity), the rebalancing cell was switched off. Otherwise, the rebalancing was activated again. By implementation of the automatized rebalancing system, an alkaline AORFB that was based on ferrocyanide and 2,6-dihydroxyanthraquinone was operated during 888 cycles and 579.6 h without any fading of capacity (and without an Ar-filled glovebox). The rebalancing system not only balance SOC, but it also balances the pH changes due to the occurrence of irreversible side reactions in the anolyte. At lab scale, our method is a suitable approach when i) redox species accelerate faster in the complete absence of air, e.g. DHAQ or long-term pH changes can affect the stability of the compounds, ii) the redox potential of the active species is very negative leading to the occurrence of HER iii) complete sealing of the flow systems is not achieved. The extraordinarily high capacity retention (100%) over 3 weeks indicates that ferrocyanide seems to be electrochemically stable in alkaline media in our system. Although this work demonstrates the feasibility of the automatized system to address the major challenge of Faradaic imbalance due to unavoidable leakage of oxygen in the anolyte, additional efforts will be required. Specifically, more robust and easy-to-implement strategies to monitor in-real-time the state-of-health of the RFB, as they could be used as a better input for the PLC to switch on/off the rebalancing system, thus more suitable for commercial applications.

Experimental Section

Chemicals. All common reagents and solvents were purchased from Aldrich (2,6-diaminoanthraquinone, KOH $\geq 85\%$,) or Alfa-Aesar (sulfuric acid and sodium nitrite, potassium ferrocyanide and ferricyanide powders (99.9–100% mesh) and used as received

Research Article
doi.org/10.1002/batt.202400086
Chemistry Europe
European Chemical Societies Publishing

without further purification. The resin used for 3D printing the cell was a UV transparent resin (Anycubic).

Preparation of the electrolytes. DHAQ//$K_4Fe(CN)_6$ – flow battery. In the flow cell reactor, the anolyte was prepared by dissolving 0.2 M 2,6-dihidroxyanthraquinone (2,6-DHAQ) in 15 mL of 1.4 M KOH. The catholyte was prepared by dissolving 0.3 M $K_4Fe(CN)_6$ in 13 mL of 1 M KOH. Detailed information about the synthesis of 2,6-DHAQ is provided in the Supporting Information, section S2. Symmetric $K_3Fe(CN)_6$//$K_2Fe(CN)_6$ flow cell. The anolyte was prepared by dissolving 0.2 M $K_3Fe(CN)_6$ and 0.1 M $K_4Fe(CN)_6$ in 45 mL of 1 M KOH, and the catholyte using 0.3 M K_4 $Fe(CN)_6$ in 13 mL of 1 M KOH.

Redox flow battery. This study uses a battery reactor formed by a two filter-pressed flow semi-cells using Nafion NRE-212 (Ion Power, USA) as the ion selective membrane, graphite felt (SIGRACELL GFD 2,5 EA, SGL Carbon) as the electrode and expanded graphite (bipolar plate SIGRACELL TF6, SGL Carbon) as the current collector. Viton® gaskets of 2- and 1- mm thickness were used for the batteries and the cell respectively due to its resistance to alkaline conditions. The projected area of the cell was 10 cm^2. A MasterFlex L/S peristaltic pump was used to provide a flow rate of 35 $mL\,min^{-1}$.

Electrochemical characterization. Charge-discharge cycles on the battery were conducted using a Neware BTS4000. The current density used was ± 30 $mAcm^{-2}$ with voltage limits of $+1.6$ V for charge and $+0.5$ V for discharge.

Rebalancing system. A rebalancing membrane-free flow device was used. Dimensions of the expanded graphite were 3×2 cm. The platinum filament diameter was 0.5 mm and had a 99.95 % purity. For the control loop, an PLC M–Duino 38R from Industrial Shields was selected. For the OCV reading, an ADC ADS1115 breakout board from Adafruit was connected to the PLC. The rebalancing device was controlled by one of output relays of the PLC, which applied a dedicated 1.2 V fixed voltage to the device when closed.

Supporting Information

The authors have cited additional references within the Supporting Information.[37,38]

Acknowledgements

The authors acknowledge financial support by the Spanish Government (Ministerio de Ciencia e Innovación, Grants PID2020-115789GB-C21 and PID2021-124974OB-C22) and Ramón y Cajal award (RYC2018-026086-I) as well as the MeBattery project. MeBattery has received funding from the European Innovation Council of the European Union under Grant Agreement no. 101046742. This work was supported by the Regional Government of Castilla y Leon (Junta de Castilla y León), the Ministry of Science and Innovation MICIN and the European Union NextGenerationEU/PRTR (C17.I1).

Conflict of Interests

The authors declare no conflict of interest.

Data Availability Statement

The data that support the findings of this study are available from the corresponding author upon reasonable request. The program code for the PLC is included in the Supporting Info.

Keywords: Flow Batteries · Cycling lifespan · Faradaic imbalance · Oxygen evolution reaction · PLC

[1] W. A. Braff, J. M. Mueller, J. E. Trancik, *Nat. Clim. Change* **2016**, *6*, 964–969.
[2] Z. Zhu, T. Jiang, M. Ali, Y. Meng, Y. Jin, Y. Cui, W. Chen, *Chem. Rev.* **2022**, *122*, 16610–16751.
[3] A. Malhotra, B. Battke, M. Beuse, A. Stephan, T. Schmidt, *Renewable Sustainable Energy Rev.* **2016**, *56*, 705–721.
[4] E. Sánchez-Díez, E. Ventosa, M. Guarnieri, A. Trovò, C. Flox, R. Marcilla, F. Soavi, P. Mazur, E. Aranzabe, R. Ferret, *J. Power Sources* **2021**, *481*, 228804.
[5] P. Alotto, M. Guarnieri, F. Moro, *Renewable Sustainable Energy Rev.* **2014**, *29*, 325–335.
[6] P. Arevalo-Cid, P. Dias, A. Mendes, J. Azevedo, *Sustain. Energy Fuels* **2021**, *5*, 5366–5419.
[7] L. F. Arenas, C. Ponce de León, F. C. Walsh, *Curr. Opin. Electrochem.* **2019**, *16*, 117–126.
[8] M. J. Watt-Smith, R. G. A. Wills, F. C. Walsh, E. Ventosa, E. Sánchez-Díez, in *Encyclopedia of Electrochemical Power Sources* (Ed.: J. Garche), Elsevier, **2009**, pp. 438–443.
[9] B. N. Arribas, R. Melício, J. G. Teixeira, V. M. F. Mendes, *Renewable Energy and Power Quality Journal* **2016**, *1*, 1025–1030.
[10] G. Kear, A. A. Shah, F. C. Walsh, *Int. J. Energy Res.* **2012**, *36*, 1105–1120.
[11] K. Lourenssen, J. Williams, F. Ahmadpour, R. Clemmer, S. Tasnim, *J. Energy Storage* **2019**, *25*, 100844.
[12] P. Leung, A. A. Shah, L. Sanz, C. Flox, J. R. Morante, Q. Xu, M. R. Mohamed, C. Ponce de León, F. C. Walsh, *J. Power Sources* **2017**, *360*, 243–283.
[13] G. Kwon, Y. Ko, Y. Kim, K. Kim, K. Kang, *Acc. Chem. Res.* **2021**, *54*, 4423–4433.
[14] E. S. Beh, D. De Porcellinis, R. L. Gracia, K. T. Xia, R. G. Gordon, M. J. Aziz, *ACS Energy Lett.* **2017**, *2*, 639–644.
[15] A. Adeniran, A. Bates, N. Schuppert, A. Menon, S. Park, *J. Energy Storage* **2022**, *56*, 106000.
[16] J. M. Fontmorin, S. Guiheneuf, T. Godet-Bar, D. Floner, F. Geneste, *Curr. Opin. Colloid Interface Sci.* **2022**, *61*, 101624.
[17] D. G. Kwabi, Y. Ji, M. J. Aziz, *Chem. Rev.* **2020**, *120*, 6467–6489.
[18] E. M. Fell, D. De Porcellinis, Y. Jing, V. Gutierrez-Venegas, T. Y. George, R. G. Gordon, S. Granados-Focil, M. J. Aziz, *J. Electrochem. Soc.* **2023**, *170*, 070525.
[19] T. Páez, A. Martínez-Cuezva, J. Palma, E. Ventosa, *J. Power Sources* **2020**, *471*, 228453.
[20] M. A. Goulet, L. Tong, D. A. Pollack, D. P. Tabor, S. A. Odom, A. Aspuru-Guzik, E. E. Kwan, R. G. Gordon, M. J. Aziz, *J. Am. Chem. Soc.* **2020**, *141*, 8014–8019.
[21] O. Nolte, I. A. Volodin, C. Stolze, M. D. Hager, U. S. Schubert, *Mater. Horiz.* **2021**, *8*, 1866–1925.
[22] T. Kong, J. Liu, X. Zhou, J. Xu, Y. Xie, J. Chen, X. Li, Y. Wang, *Angew. Chem. Int. Ed.* **2023**, *62*, DOI 10.1002/anie.202214819.
[23] M. Nourani, C. R. Dennison, X. Jin, F. Liu, E. Agar, *J. Electrochem. Soc.* **2019**, *166*, A3844.
[24] R. Rubio-Presa, L. Lubián, M. Borlaf, E. Ventosa, R. Sanz, *ACS Materials Lett.* **2023**, *5*, 798–802.
[25] T. Páez, A. Martínez-Cuezva, J. Palma, E. Ventosa, *ACS Appl. Energ. Mater.* **2019**, *2*, 8328–8336.
[26] B. H. Robb, T. Y. George, C. M. Davis, Z. Tang, C. H. Fujimoto, M. J. Aziz, M. P. Marshak, *J. Electrochem. Soc.* **2023**, *170*, 30515.
[27] W. Liu, Z. Zhao, T. Li, S. Li, H. Zhang, X. Li, *Sci Bull (Beijing)* **2021**, *66*, 457–463.
[28] R. Pichugov, P. Loktionov, A. Pustovalova, A. Glazkov, A. Grishko, D. Konev, M. Petrov, A. Usenko, A. Antipov, *J. Power Sources* **2023**, *569*, 233013.
[29] N. Poli, A. Trovò, P. Fischer, J. Noack, M. Guarnieri, *J. Energy Storage* **2023**, *58*, 106404.

[30] K. E. Rodby, T. J. Carney, Y. Ashraf Gandomi, J. L. Barton, R. M. Darling, F. R. Brushett, *J. Power Sources* **2020**, *460*, 227958.
[31] A. Q. Pham, O. K. Chang, *US 8,916,281 B2*, **2014**.
[32] N. Poli, M. Schäffer, A. Trovò, J. Noack, M. Guarnieri, P. Fischer, *Chem. Eng. J.* **2021**, *405*, 126583.
[33] Y. Jing, E. W. Zhao, M. A. Goulet, M. Bahari, E. M. Fell, S. Jin, A. Davoodi, E. Jónsson, M. Wu, C. P. Grey, R. G. Gordon, M. J. Aziz, *Nat. Chem.* **2022**, *14*, 1103–1109.
[34] M. Hu, A. P. Wang, J. Luo, Q. Wei, T. L. Liu, *Adv. Energy Mater.* **2023**, *13*, 2203762.
[35] T. Páez, A. Martínez-Cuezva, R. Marcilla, J. Palma, E. Ventosa, *J. Power Sources* **2021**, *512*, 230516.
[36] A. L. Shestakov, A. V. Keller, in *Journal of Physics: Conference Series 1864 012073*, **2021**.
[37] R. Sanz, C. Sedano, *ES2819599 A1*, **2021**.
[38] Atmel, "AVR121: Enhancing ADC resolution by oversampling Features," can be found under http://ww1.microchip.com/downloads/en/AppNotes/doc8003.pdf, **2005**.

Manuscript received: February 6, 2024
Revised manuscript received: May 10, 2024
Accepted manuscript online: May 14, 2024
Version of record online: June 24, 2024